ESD-TR-70-98

Technical Report

477

Incoherent Scatter Measurements of F-Region Density, Temperatures, and Vertical Velocity at Millstone Hill

J. V. Evans
R. F. Julian
W. A. Reid

6 February 1970

Prepared for the Office of the Chief of Research and Development, Department of the Army
under Electronic Systems Division Contract AF 19(628)-5167 by

Lincoln Laboratory

MASSACHUSETTS INSTITUTE OF TECHNOLOGY

Lexington, Massachusetts

MASSACHUSETTS INSTITUTE OF TECHNOLOGY
LINCOLN LABORATORY

INCOHERENT SCATTER MEASUREMENTS OF F-REGION DENSITY, TEMPERATURES, AND VERTICAL VELOCITY AT MILLSTONE HILL

J. V. EVANS
R. F. JULIAN
W. A. REID

Group 21

TECHNICAL REPORT 477

6 FEBRUARY 1970

LEXINGTON MASSACHUSETTS

The work reported in this document was performed at Lincoln Laboratory, a center for research operated by Massachusetts Institute of Technology. The work is sponsored by the Office of the Chief of Research and Development, Department of the Army; it is supported by the Advanced Ballistic Missile Defense Agency under Air Force Contract AF 19(628)-5167.

ABSTRACT

The Millstone Hill Thomson (incoherent) scatter radar system has been operated routinely since 1963 to perform a synoptic study of F-region electron densities, and electron and ion temperatures. This report describes system changes made in 1968 which considerably increased the accuracy of the measurements and allowed their extension to higher altitudes. These changes have also made it possible to measure the vertical velocity of the plasma over the altitude range 450 to 900 km to an accuracy on the order of 5 to 10 m/sec, depending upon altitude and time of day.

Of even greater significance, complete machine reduction of the results is now possible so that considerable savings in time and effort have been secured in analyzing the data. The new system permits all the radar data to be gathered in the digital computer in real time, thereby eliminating the need for post real-time processing of magnetic-tape recordings of the signals. Furthermore, it is now possible to transmit the data to other workers in computer-usable form.

This report describes the main functions of the computer program required to analyze the measurements, and lists the times of all measurements made with the new system prior to 1 January 1970. Examples of these results are presented and discussed.

Accepted for the Air Force
Franklin C. Hudson
Chief, Lincoln Laboratory Office

CONTENTS

INCOHERENT SCATTER MEASUREMENTS OF F-REGION DENSITY, TEMPERATURES, AND VERTICAL VELOCITY AT MILLSTONE HILL

I. INTRODUCTION

A vertically directed incoherent scatter radar system operating at 68-cm wavelength (440 MHz) was brought into operation at Millstone Hill, Westford, Massachusetts (42.6°N, 71.5°W) in 1963.[1] This radar system has since been in routine use securing measurements of F-region electron density, and electron and ion temperatures. The results obtained during 1963 through 1965 have been published in earlier technical reports as well as in a number of journal articles listed in Table I.

TABLE I

PUBLICATIONS CONCERNING THE MILLSTONE HILL UHF (68-CM WAVELENGTH) THOMSON SCATTER RESULTS

Year	Manths Covered	Publicotian
1963	March, July, August, September	Ref. 2
	December, April, July, Navember	Ref. 3
	February 1963 to January 1964	Technical Repart 374, Lincaln Laboratary, M.I.T. (22 January 1965), DDC AD-616607
1964	April, July, Navember	Ref. 4
	January thraugh December	Technical Report 430, Lincaln Laboratory, M.I.T. (15 Navember 1967), DDC AD-668436
1965	Jonuory, April, August	Ref. 5
	January thraugh December	Technical Repart 474, Lincoln Laboratary, M.I.T. (8 December 1969)

The determination of the electron and ion temperatures at a given altitude depends upon a spectrum analysis of the signals returned from that altitude. Prior to 1968, we accomplished this with a spectrum analyzer that could examine only a single height at a time. Accordingly, throughout the period January 1965 to July 1968, we used a magnctic-tape recorder to store the received signals for later analysis. In this way, a considerable increase in the time resolution could be achieved, but it was necessary to spend a great deal of time in processing the magnetic tapes. This scheme had other serious drawbacks – most notably, the separation of the results

for density and temperature made it necessary to perform the final stages of data reduction by hand; this proved to be most time consuming and unattractive work.

Beginning in 1966, we seriously considered the construction of a spectrum analyzer that could examine the signals from all altitudes of interest at the actual time of receipt, i.e., in real time. We also considered it desirable that the integration of these signal samples be drift-free, and yield results that could be stored in the digital computer along with the measurements from which the electron density is determined. In 1967, we began the construction of a system capable of performing these tasks, and were able to place it into operation in July 1968.

In Sec. II, the new spectrum analyzer is described, as well as the other changes that have been made to the equipment since it was first brought into operation.[1] Section III describes the operating procedure for the radar equipment developed since July 1968 that provides semiautomatic control of the system; also given in this section are tables of times for which measurements have been made prior to 1 January 1970. The functions of the computer program that has evolved to handle the data analysis are described in Sec. IV. Development of this program required considerable effort, and took at least as long as the development of the new spectrum analyzer. Section V presents and discusses briefly some results produced by the new system.

II. EQUIPMENT

A. System Parameters

The main features of the incoherent scatter radar system have been described previously.[1,2] Although numerous changes and improvements have been made to the equipment since it was brought into operation, the system parameters have not changed appreciably – with the exception of the noise temperature of the radar receiver, which has been lowered. Table II lists the parameters of the system as of 1 January 1970.

TABLE II
RADAR SYSTEM PARAMETERS AS OF 1 JANUARY 1970

Antenna diameter	220 feet
Antenna collecting area	~1600 m^2
Polarization	
Transmitted	Circular
Received	Opposite sense circular
Peak transmitter power	3.0 MW maximum
Average transmitter power*	120 kW maximum
Pulse length (See Table IV)*	2.0 msec maximum
System temperature*	~180°K
Receiver pre-detector bandwidth†	40 kHz
Receiver post-detector time constant†	50 μsec for 100-μsec pulses 200 μsec for 0.5-, 1.0-, and 2.0-msec pulses

* Manitored continuously.

† For the power profile channel (Sec. II-E).

As noted in Table II, many of the system parameters are monitored continuously, and the antenna collecting area can be determined from observations of the intensity of the radio source Cygnus A which transits the beam daily. However, the measurements of electron density, electron and ion temperatures, or drift velocity do not depend upon absolute measurements of echo intensity, and the monitoring of the various parameters of the radar is undertaken solely to ensure that it is functioning properly.

B. Antenna

The radar antenna consists of a fixed vertically pointing 220-foot-diameter parabola with a focal length of 100 feet (see Ref. 1). Since its completion, the antenna has been surveyed annually and adjustments made to maintain a true parabolic contour. Some of the concrete post supports have settled, requiring that they be replaced.

Apart from this and other routine maintenance, the only changes made to the antenna system were undertaken in an attempt to minimize ground-clutter echoes. In 1967, we placed a large conical skirt around the feed horn in order to cut down the intensity of any signals transmitted toward the horizon. With this done, we considered scattering from the tripod legs of the feed support system as the largest remaining source of unwanted radiation at low angles. Accordingly, we placed absorbing netting on the insides of these legs to eliminate direct reflections. Forward scattering around the legs was still possible, however, and to reduce this it was necessary to cut down the energy incident on them. We accomplished this by constructing an extension for the feed horn that increases the taper of the illumination over the dish from 10 to 20 dB. This extension also serves to cut down the radiation at large angles by virtue of a quarter-wave choke that surrounds it. No loss of antenna gain was observed when the extension was installed – probably because the horn efficiency was raised by the presence of the choke.

Although these changes have not eliminated ground-clutter echoes, they have lowered their intensity, and it is no longer necessary to blank the receiver out to ranges (~150 km) where the last echoes occur. Indeed, the clutter echoes do not now saturate the receiver, so that it is possible to attempt to remove them in the data processing; we are developing programs that attempt to do this.

C. Receiver

The receiver system is a straightforward multiple superheterodyne, having intermediate frequencies of 30 and 2.0 MHz, that is preceded by a parametric amplifier. All the local-oscillator frequencies are derived from the station master oscillator to achieve good frequency stability. This is required for measurement of the vertical drift velocity of the plasma (Sec. IV-D).

The original receiver preamplifier was an electron-beam parametric amplifier (Adler tube) that was synchronously pumped. This device gave extremely reliable service, and was essentially immune to large amounts of RF leakage from the transmitter. Synchronous pumping (at 880 MHz) yielded the lowest system noise, but folded the radar signals about their center frequency and made it impossible to search for frequency shifts produced by drifts. In 1967, the Adler tube was replaced by a regenerative diode-parametric amplifier operating at ambient temperature and employing a klystron oscillator to supply pump power. This amplifier yields a lower system temperature (Table II) as well as eliminating the fold-over problem. The vacuum tube receiver has been replaced by a completely "solid-state" receiver in which gating is accomplished with commercially available diode gates. With the possible exception of the parametric

amplifier, the new system has greater gain stability than the old system. On the other hand, the parametric amplifier has been found to be somewhat temperature sensitive. Day-to-night temperature changes in the hut (under the antenna) in which the amplifier is located required that it be retuned several times during a 24-hour period. By improving the thermal insulation and air conditioning the hut, this problem has largely been remedied.

A predetector bandwidth of 40 kHz is employed in the receiver, and this is set by a filter placed in the 2-MHz IF channel. Unlike the earlier system, this same bandwidth is employed for all pulse lengths, and only the post-detector time constant is varied (Table II).

The receiver system temperature is continuously monitored by including in the sweep integration process a calibration pulse consisting of a known amount of RF noise power inserted at the receiver terminals via a directional coupler. This noise pulse also serves to establish the absolute power in the echoes.

D. Transmitter

The transmitter has not been modified significantly since it was built. However, we recently replaced the vacuum tube exciter with one employing solid-state components. This exciter is a reverse superheterodyne employing the same intermediate frequencies as the receiver. Mutual interference is kept to a minimum by extensive screening, and by maintaining all signals at low power levels until the final frequency of 440 MHz is reached.

Although the transmitter is rated at 150-kW average power output, we have found that it is not usually possible to exceed 130-kW output before the maximum permissible beam current is reached. At the low duty cycle employed in many of the measurements, it is possible to achieve a peak power of 3 MW, i.e., exceeding the 2.5-MW rating of the transmitter. However, no adverse effects have been encountered operating at this peak power.

E. Power Profile Channel

Measurements of the distribution of echo power with range are made by means of sweep integration using a digital computer.[1] This measurement is termed the power profile and leads to a determination of the electron density distribution with altitude.

Power profile measurements are carried out by sampling the receiver output repeatedly at equal intervals along the timebase, and summing together all samples taken at the same position on successive sweeps. For this purpose, the 2-MHz IF signals are converted in frequency to 200 kHz and then applied to a linear rectifier and sampled.

The rectifier is designed to be linear over the range 0.1 to 10 volts, and is followed by an LC low-pass filter. Two low-pass filters are available having time constants of 50 and 200 μsec. Selection between them is carried out by a relay. The filtered rectified signal is applied to an analog-to-digital converter, possessing 1024 levels, that operates over a range of 10 volts. For observations made with 0.1-msec pulses, samples are taken at 50-μsec intervals, and the 50-μsec low-pass filter is used. For all other pulse lengths, the sample spacing and low-pass filter time constant are 200 μsec (Sec. III-A). Samples accepted by the computer are immediately squared before being summed. In this way, a true square-law rectification process is achieved with a dynamic range of the order of 50 dB.

F. New Spectrum Analyzer

1. Limitations of Original System

The most significant change made to the equipment has been the construction of a new spectrum analyzer. This has made a considerable improvement in the accuracy of the results, as well as rendering all the data analysis open to machine processing as noted in the Introduction (Sec. I). The original spectrum analyzer and later modifications have been described elsewhere.[1,5] Basically, these systems employed a bank of narrow-band crystal filters to analyze a sample of the received signals gated from the radar timebase. The duration of the sample was made equal to the length T of the transmitted pulse, and the delay t was chosen to correspond to a height of interest. The filter outputs were rectified and stored in analog (Miller) integrators.

This scheme suffered a number of drawbacks. It was possible to examine only a single delay at a time, and thus to analyze echoes from all heights of interest required about 90 minutes observing time. In order to reduce this, we began in 1965 to record the IF signals on magnetic tape for later playback and analysis.[5] This proved to be a time-consuming operation since approximately 2 to $2\frac{1}{2}$ weeks were needed to process the tapes obtained in a single 24-hour period. Although we followed the best possible construction practice available at the time, the analog integrators were subject to DC drifts that served to introduce "noise" into the measurements. As a result, the maximum useful length of an integration period was limited to about 5 minutes, so that the minimum signal-to-noise ratio for which useful measurements could be obtained was about 0.1.

A further limitation was imposed by the filters themselves, which did not have equal response above and below the peak transmission. As a result, the spectra obtained were asymmetric about the radar frequency, and it was necessary to average the two sides to remove the effect.[5] Finally, the spectrum analyzer constituted a large piece of electronic equipment requiring constant attention and maintenance.

2. First Plan for New System

In searching for a replacement for the system described above, we sought an approach that would have the following characteristics:

(a) Examine all heights of interest simultaneously,

(b) Provide accurate drift-free integration,

(c) Operate in real time (i.e., eliminate analog data storage),

(d) Place the spectrum results in the computer along with the corresponding power profile results.

A scheme which achieves these goals has been developed at the Arecibo Observatory by Perkins and Wand.[6] In this scheme, the spectrum analysis of the signals is carried out by forming the autocorrelation function of successive samples of the signals, and then obtaining the Fourier transform. Thus, for example, to obtain the spectra of signals observed with a T = 0.5-msec pulse, samples of the received signals are taken at 20-μsec intervals over a 0.5-msec interval of the timebase, and the autocorrelation function of these samples is determined in a digital computer. If carried out in full, this requires the computer to perform 3236 multiply operations for every 0.5-msec interval examined. Savings may be made, however, if not all the lagged products are formed. In the limit, only 26 multiply operations are needed to form one sample of each of the possible lagged products 0, 20, 40, . . . , 500 μsec. Perkins and Wand call this the "single"

sample" method, and employ this approach to examine altitudes for which the pre-detector signal-to-noise ratio is expected to be large, i.e., where the samples are highly correlated so that it is unnecessary to form all possible products. They estimate[6] that the loss in accuracy under these circumstances is equivalent to reducing the observing time by about a factor of four. Thus, by reducing the number of multiply operations per correlation function to 26, it is possible to examine a large number of altitudes simultaneously at the loss of a certain amount of time resolution. A similar tradeoff may be had by adopting the "one-bit" correlator approach as discussed by Farley.[7]

At Millstone, the signal-to-noise ratio is less than unity at many heights of interest. Under these circumstances, the accuracy of the correlation method depends on the square root of the number of lagged products that are formed,[8] so that the single-sample method is no longer acceptable. Accordingly, we decided that the full autocorrelation function would be computed. In order to perform all the necessary multiply operations, we secured a parallel multiply unit for the station SDS 9300 computer. This unit was designed to perform twelve multiplications in the cycle time of one. Unfortunately, delays in making both the hardware and software parts of the system perform properly were encountered, and a cut in the funds available to support the radar site forced us to return the unit to the manufacturer before it could be brought into operation for ionospheric studies. The recent development of the Cooley-Tukey algorithm for fast spectrum analysis[9] has made the approach described here considerably more practical, and a number of groups have now constructed fast digital processors for performing spectrum analysis calculations.

3. Second Plan for New System

Recognizing that the digital autocorrelation method might encounter difficulties, we devised an alternate scheme that was somewhat less ambitious and seemed sure to work. As it transpired, this second plan was the one we put into effect. In order to examine several height intervals simultaneously, the number of integrators available must be increased. Therefore, it seemed logical to employ the digital computer to perform the task of signal integration, while using analog elements to analyze the spectra of the signals. If the gated-receiver approach were used, a separate filter bank would be required for each height examined. However, by applying the signals continuously to a bank of wide filters, acceptable height and frequency resolution can be achieved when the filter bandwidth b is given by

$$b = I/T \qquad \text{Hz} \tag{1}$$

where T is the pulse length (seconds). The optimum height and frequency resolution are obtained when the power-vs-frequency response of the filter is matched to that of the energy in the pulse. That is, for square pulses the voltage response of the filter should be of the form

$$v(f) = v(f_o)\left[\frac{\sin 2\pi T(f - f_o)}{2\pi T(f - f_o)}\right] \tag{2}$$

where f_o is the filter center frequency. When this is the case, the observed spectrum is identical to that obtained with a gated receiver and very narrow filters. Specifically, the measured power at a frequency f_o is

$$P(f_o) = \int_{-}^{+} W(f)_t j(f - f_o)\, df \tag{3}$$

where $W(f)_t$ is the fluctuation spectrum of the scattering plasma at delay t. The convolution function $j(f - f_o)$ is

$$j(f - f_o) = \frac{2}{\pi T(f - f_o)^2} \left[1 - \frac{\sin 2\pi T(f - f_o)}{2\pi T(f - f_o)}\right] \quad . \tag{4}$$

The success of this approach depends critically upon the availability of filters that have characteristics close to Eq. (2). Fortunately, multipole crystal filters can now be designed using computer programs, so that suitable filters are commercially available.

The chief difficulty that could be encountered with the filter bank approach is that it is necessary to take a large number of samples at the filter outputs simultaneously, and then enter these into the computer serially. The problem can be avoided if the signals applied to the filters are themselves delayed with respect to each other, thereby permitting the outputs to be sampled one at a time.

4. Realization of Spectrum Analyzer

Figure 1 provides a block diagram of the scheme adopted for the new spectrum analyzer. The IF signals are applied to a tapped delay line. Each tap drives one of 24 filters that form the matched-filter bank. Arrangements are made to sample the filter outputs via a switch (S_1 in Fig. 1) at the same rate as the signals propagate down the delay line. In our system, an acoustic delay line is employed and the pickup coils are spaced to apply replicas of the IF signals to the filters with a relative delay of 20 μsec. Switch S_1 consists of 24 balanced-diode gates that are opened in sequence, one at a time, for 20 μsec by a clocked-digital shift-register. Thus, in order to sample 24 filters, an interval of 480 μsec is required. This allows a separate spectrum to be obtained every 0.5 msec along the timebase.

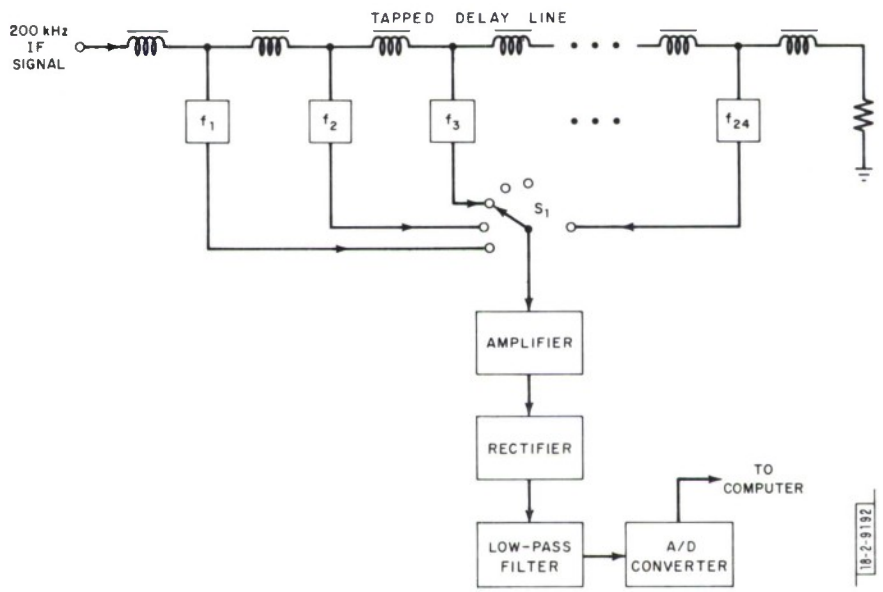

Fig. 1. Block diagram of new spectrum analyzer scheme.

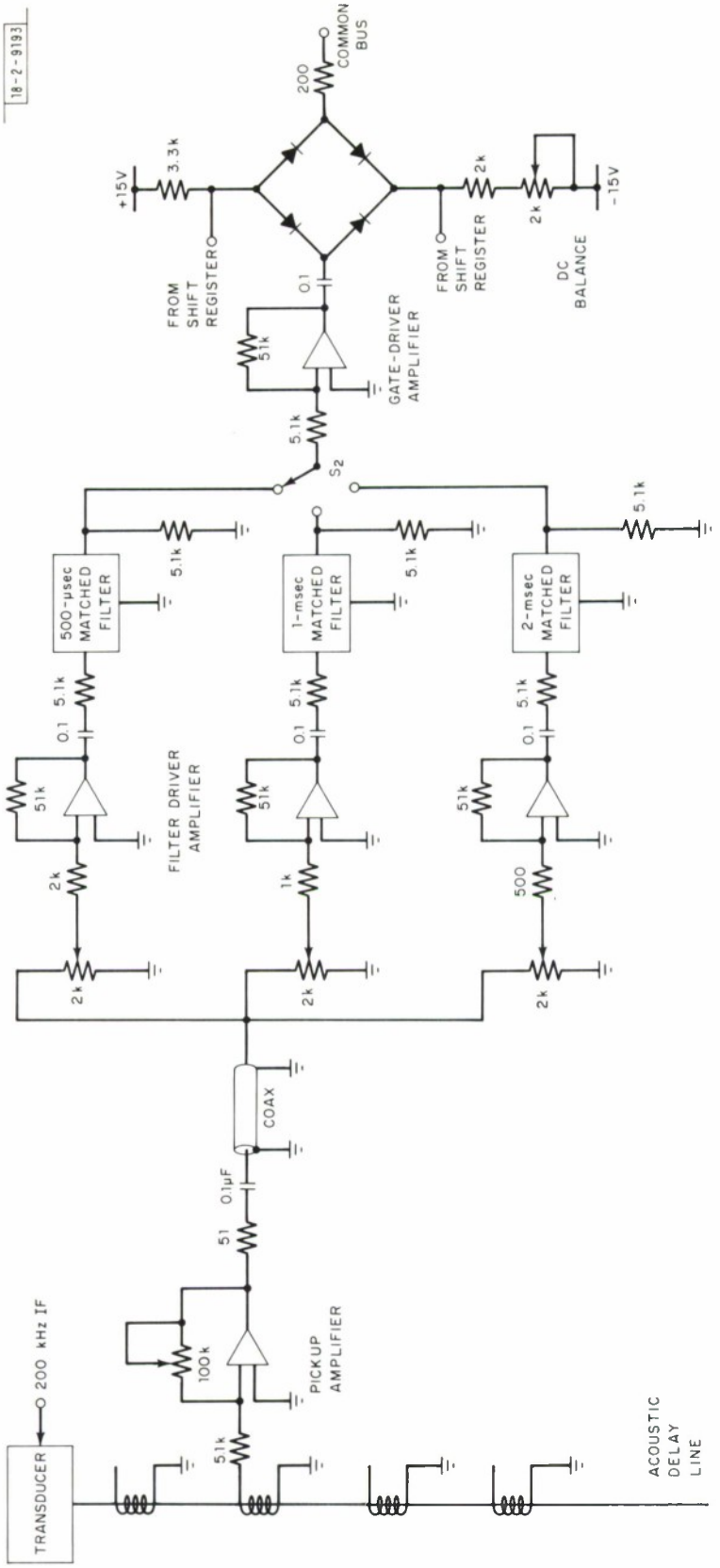

Fig. 2. Diagram of filter network at each tap.

The principal drawback of this scheme is that a separate filter bank is required for each of the pulse lengths used. Thus, two new filter banks were purchased to suit 0.5- and 1.0-msec pulse observations; for 2.0-msec measurements, a third bank was assembled using the old 500-Hz filters employed in the original spectrum analyzer.

5. Filter Networks

Figure 2 shows one of the 24 filter networks employed in the spectrum analyzer. Each pickup coil on the delay line drives a pickup amplifier whose gain is adjustable. In this way, the attenuation of the signals down the delay line can be compensated. The pickup amplifier drives three independent amplifiers that are coupled to the three filters (matched to 0.5-, 1.0-, and 2.0-msec pulses) via attenuators. The gains of these amplifiers differ so that the mean noise voltage appearing at the filter outputs is approximately the same (i.e., independent of the bandwidth). The filters are driven continuously and a relay-operated switch (S_2 in Fig. 2) selects the filter in use. After further amplification, the signals are applied to the diode gates that act as the selector switch (S_1 in Fig. 1). Each diode gate is normally held closed by a flip-flop. When allowed to open, a current of about 5 mA flows through the diodes. This limits the peak RF signal that can be driven through the gate to 0.005R volts, where R is the output resistance. To reduce the effects of DC offsets and switching transients, R is made as small as possible (actually 400 ohms) consistent with being able to obtain 10 volts peak detected output. The diode bridges can be balanced to yield zero output when no signal is applied.

6. Frequency Control

In order to obtain suitable filters, we were obliged to employ center frequencies in the vicinity of 200 kHz. Accordingly, two identical banks of 12 filters were obtained for each pulse length. These filters have center frequencies spaced at 2-kHz intervals and span the interval 188 to 210 kHz. Each filter bank is driven by a separate receiver channel, as shown in Fig. 3. In this way, by adjusting the 2-MHz to 200-kHz local-oscillator (LO) frequencies, the filters can be moved to cover different intervals. For UHF observations, the filters are interlaced to yield measurements at 1-kHz intervals, i.e., the spectrum analyzer is adjusted to examine the echoes at $-11.5, -10.5, -9.5, \ldots, -0.5, +0.5, \ldots, +11.5$ kHz with respect to the radar frequency. The spectrum analyzer can also be employed with the L-band radar and, in this case, the filter banks are placed end to end, i.e., the range -23 to $+23$ kHz with respect to the radar frequency is examined at 2-kHz intervals. Table III gives the LO frequencies required for these settings.

Figure 3 shows that the odd-numbered filters (spanning $-11.5, -9.5, \ldots, +10.5$ kHz at UHF) are driven with replicas of the signal delayed at $20, 40, \ldots, 240$ μsec. In order that the even filters (covering $-10.5, -8.5, \ldots, +11.5$ kHz) be driven at later delays, a fixed length of delay line introducing 240-μsec delay is employed. The attenuation introduced by this additional piece of line is 35 dB, requiring that an additional driver amplifier be interposed between it and the tapped delay line it feeds.

In operation, we found that the two separate mixers (Fig. 3) could not be made identical, with the result that the spectra obtained yielded points that were alternately high and low. Despite several attempts at improving the mixers this problem could not be eliminated, and we decided to commutate the mixer outputs; this is done under the control of the computer every m sweeps of the timebase (m is usually set at 750). This commutation exchanges the roles of the even and odd filters, and the computer keeps track of the correct filter center frequencies when summing

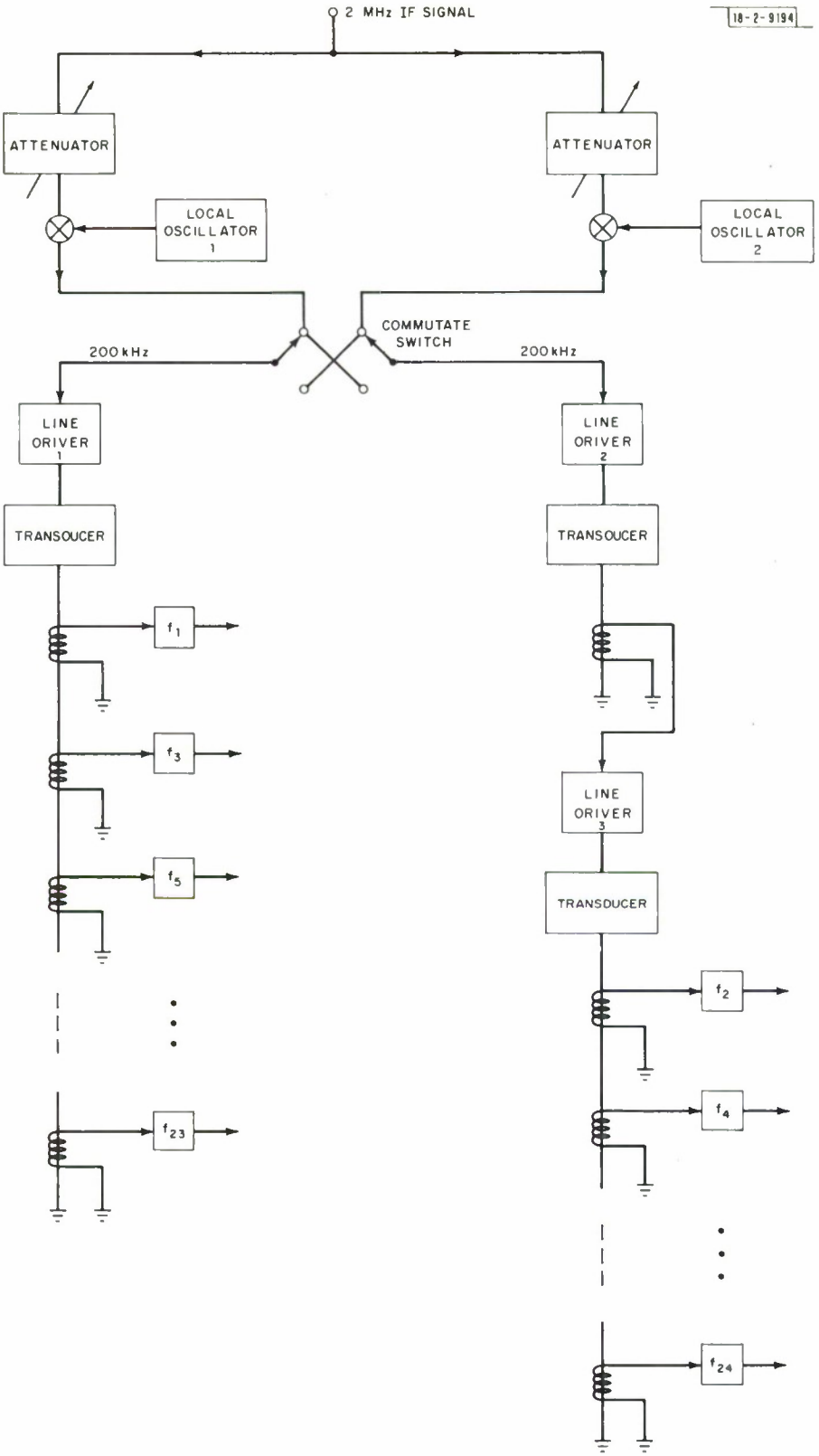

Fig. 3. Arrangement of delay-line system.

TABLE III

LOCAL-OSCILLATOR FREQUENCIES EMPLOYED IN THE SPECTRUM ANALYZER

Mode		Local Oscillator 1 (MHz)	Local Oscillator 2 (MHz)
UHF	Normal	1.8005	1.8015
	Transposed	2.1995	2.1985
L-band	Normal	1.789	1.813
	Transposed	2.211	2.187

the samples. This modification successfully eliminated effects due to dissimilarity of the mixers. We then found that the spectra exhibited an asymmetry; typically, one side would be somewhat stronger than the other. This is attributable to unequal responses of the filters in their skirts. Accordingly, we decided to transpose the filters about the radar frequency, and this was carried out by switching the LO frequencies from below 2 MHz to an equal amount above (Table III). In effect, the filters are electrically reflected about the radar frequency since they are employed to examine alternately the high and low sidebands of the spectrum. Commutating the LO frequencies in this way is performed every 2 m sweeps.

These changes cause each filter to be employed at four different places in the spectrum; conversely, each point in the spectrum is derived from samples taken from four physically separate filters. By employing the computer to perform the commutating and keep track of it, the addition of the samples can proceed in such a way that any true asymmetry in the spectrum is preserved. That is, this switching serves only to eliminate instrumental effects.

7. Rectifier and Sampling

Figure 4 shows the rectifier system employed to sample the filter outputs. In order that the rectifier can respond within 20 μsec to the full value of the envelope of the signal, it must have a wide bandwidth and be followed with a time constant that is short compared with 20 μsec. Unfortunately, as noted above, we were obliged to purchase filters operating at ~200 kHz so that the rectifier can sample, at most, four cycles of the waveform. By employing a full-wave rectifier, the period of the ripple applied to the low-pass filter is reduced to 2.5 μsec, and a time constant

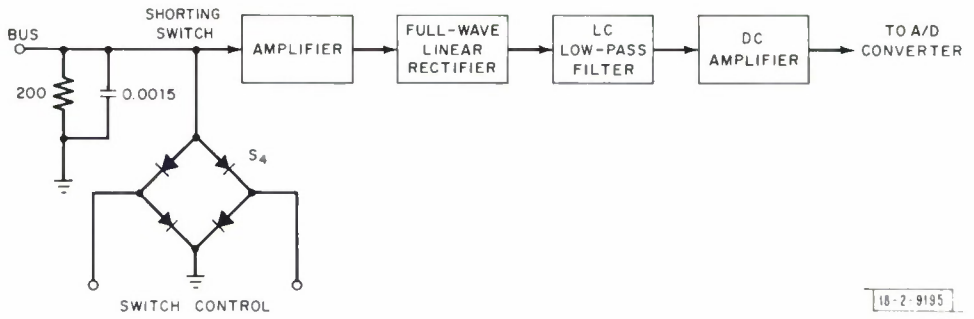

Fig. 4. Rectifier system.

of 7 μsec (the geometric mean of 2.5 and 20 μsec) was found to be an acceptable compromise. As in the power profile channel, a linear rectifier is employed which drives a 10-bit analog-to-digital converter operating over a 10-volt range. These samples of signal voltage are squared in the computer.

We found that the electronic switch S_1 (Fig. 1) introduced noise or transients whenever the digital shift-register was clocked. These transients could not entirely be removed by filtering at the rectifier output, owing to the requirement that the time constant be less than 20 μsec. Considerable improvement was obtained by filtering at the input (Fig. 4), and by using a second diode gate to connect the input to the rectifier to ground for a period of 5 μsec centered on the clock time. This lowered the available sample time to 15 μsec, but reduced the switching noise to the level of the least-significant bit in the A/D converter. The 5-μsec dead period also is necessary to permit the low-pass filter to discharge between samples, otherwise energy from one sample can be carried over into the next. Sampling of the spectrum channel is carried out at the end of the 15-μsec sample window, i.e., immediately before the input to the rectifier is shorted (by S_4 in Fig. 4). The timing of this chain of sample pulses is adjusted to allow for the overall delay in the receiver, filter, and rectifier to yield samples that are precisely controlled in delay with respect to the leading edge of the transmitter pulse. That is, to obtain a spectrum at a nominal delay of 1.5 msec, the first sample is taken approximately 2.1 msec following the transmitter pulse.

G. Timing Equipment

All events in the cycle of operations are timed by digital clocks operating from a 100-kHz standard frequency derived from the station master oscillator. Control of the transmitter pulse length, sweep interval, receiver gate position, location, and duration of the noise calibration pulse are under control of a radar timer that provides four preset options or modes. These modes are designated A through D and are selectable from the control console by push buttons. Alternatively, the timer can be placed under remote control, in which case the mode selection is performed by the computer.

III. OPERATING PROCEDURE

A. Operating Modes

As outlined in the previous section, the new equipment provides four selectable operating modes designated A through D. Relay controls select the appropriate bandwidth filters for each mode, and the time constant of the low-pass filter in the power profile channel. Table IV summarizes the operating parameters for each of these modes, and the location on the timebase of the noise calibration pulse and its width. Also given is the position and width of a portion of the timebase, beyond all ionospheric echoes and preceding the noise calibration pulse, that is sampled as a measure of the intrinsic receiver noise. In the spectrum channel, a separate spectrum is available every 0.5 msec. These are completely independent only when 0.5-msec pulses are employed (mode B), but, despite this, all possible spectra are accepted between delays on the timebase given in Table IV. An additional five independent spectra (i.e., spaced by the pulse length) are taken at large delays on the timebase (see table) to measure the noise present in each channel.

TABLE IV

PARAMETERS EMPLOYED FOR THE FOUR SELECTABLE MODES

Porometer	Mode (msec) A	B	C	D
Pulse length	0.1	0.5	1.0	2.0
Interpulse period	8.0	13.0	20.0	40.0
Receiver gate deloy*	0.5	1.5	2.0	5.0
Profile chonnel sample spacing	0.05	0.20	0.20	0.20
Profile channel time constont	0.05	0.20	0.20	0.20
Deloy to receiver noise window	5.5	9.0	12.0	17.0
Width of receiver noise window	0.5	1.0	2.0	2.0
Delay to calibration noise pulse	6.5	11.0	17.0	35.0
Width of calibrotion noise pulse	0.5	1.0	2.0	2.0
Deloy to first signal spectrum	–	1.5	3.0	6.0
Delay to lost signal spectrum	–	5.0	7.5	10.5
Delay to first noise spectrum	–	8.0	8.0†	11.0†
Delay to lost noise spectrum	–	10.5	13.0†	21.0†

* May be manually adjusted.

† Increased by 2.0 msec in February 1970.

B. Real-Time Computer Operations

A computer program has been developed that affords complete control over the experiment. Basically, the program squares and sums the signal samples available at the outputs of the power profile and spectrum channels. In the case of the power profile, it is necessary only to keep track of the positions of the samples along the timebase. However, the spectrum channel provides four separate sample sequences, depending upon whether or not the mixer outputs have been interchanged and the LO frequencies are above or below the sample frequency. For this reason, the computer controls these switching operations via an output register and associated relays. The interval between commutations is determined by counting a predetermined number of sweeps, and the duration of the entire integration period is determined in the same fashion.

All the parameters listed in Table IV, as well as the duration of the integration period, amplitude of the calibration pulse, commutation interval, date, etc., are stored in the program in a manner that makes them accessible to change via the typewriter.

When the radar timer is placed in remote control, the computer takes over the selection of the operating modes via an output register. Two options are then available. In one, the operator requests a run of a given type (A to D) by pressing the appropriate key on the typewriter; the computer then sets the radar into that mode and commences taking data at the next round 10-sec interval. The alternative is for the operator to elect an "automatic sequence" option at the commencement of the operating period. In this case, it is necessary to specify the cycle in which runs are to be carried out (i.e., the type and duration of each run before the cycle repeats).

Automatic sequencing may be interrupted to reject a particular run, change the stored parameters, or change the desired sequence. At the commencement of the first run taken following Greenwich midnight, the computer requests the operator to supply a new date.

C. F-Region Critical Frequency

An important parameter in the data processing (Sec. IV-C) is the critical frequency of the F-region determined using a C-4 ionosonde located about 1 km from the radar. In the past, this sounder has been left to operate unattended, and records were made on 35-mm film. In many instances, during radar operations, malfunctions occurred that were not discovered at the time. In order to remedy this, arrangements have been made to permit the ionosonde to be turned on from the radar console, and control of its operating frequency transferred to a local frequency synthesizer. The ionosonde receiver output may also be viewed on a local A-scope display. In this way, the operator may measure f_oF2 remotely by advancing the frequency of the synthesizer until the delay to the ordinary trace increases rapidly. These measurements of the critical frequency are stored in the computer, which requests the value of f_oF2 each time an A-mode run is reached in the mode sequence, or is requested by the operator. Film records of automatic sweeps made by the ionosonde at 30-minute intervals are also made, and, if desired, values of f_oF2 obtained from these may be used in the data analysis in place of those obtained by the radar operator.

D. Computer Output

At the end of the run period, the computer halts the integration process and partially processes the results before proceeding to the next run. These data are written on magnetic tape for later non-real-time analysis (Sec. IV), and are printed by a high-speed line printer to allow the operator to see that the experiment is proceeding satisfactorily. In the case of the power profile results, the raw computer sums are tabulated vs delay t along the timebase and presented on a monitor display. The equivalent ionospheric height h is computed according to

$$h = 150\left(t - \frac{T + \tau}{2}\right) \qquad \text{km} \tag{5}$$

where T is the transmitter pulse length, and τ is the total receiver delay (all times being in milliseconds). The computer also calculates the mean of the samples within the receiver noise window and subtracts this from all other samples. The residuals are then converted to echo temperature T_r employing the known amplitude (°K) of the calibration pulse as scale factor. Finally, an echo power profile is computed according to

$$\sigma_r = 2T_r h^2 kb \qquad \text{W km}^2 \tag{6}$$

where k is Boltzmann's constant (1.38×10^{-23} erg/°K), and b is the receiver predetector bandwidth (in hertz). The quantities h, T_r, and σ_r are also tabulated against delay t on the high-speed printout.

It may be shown that σ_r is directly related to the echo cross section per unit height in the ionosphere, and hence proportional to the electron density.[1] Accordingly, at the completion of each run, the computer also presents on the monitor display a plot of σ_r normalized to the largest value.

For the spectrum channel, the computer calculates the mean noise intensity $P_n(f)$ in each channel and subtracts this from the sums at the other delays. Finally, these residuals are divided by $P_n(f)$ to yield the signal-to-noise ratio at each delay and frequency. These values are printed out and stored on the magnetic tape.

E. Observing Program

The new equipment provides the opportunity for making observations in a variety of different ways. However, since each possible observing procedure may require a separate program to handle the data analysis, we have thus far limited the observations to two kinds. The first of these provides good coverage of the entire altitude interval 150 to 1100 km with modest time resolution (30 minutes). For this program, A-, B-, and C-mode runs are performed sequentially, each being 8 minutes in duration. A second type of observing schedule has been employed to emphasize the drift measuring capability afforded by the C-mode runs. For these observations, the sequence of runs is A, B (each 4 minutes), followed by four C-mode runs (each lasting 8 minutes). This cycle is termed "Drifts" to distinguish it from the normal or "Regular" cycle.

We have not found it profitable to include D-mode runs in either of these sequences, owing to the low signal-to-noise ratio encountered at the altitudes covered with this mode (Table IV). However, separate observations using only the D-mode are planned to search for the transition altitude between O^+ and H^+ ions, which has not been detected in the Millstone observations carried out thus far.

During the latter part of 1968, we attempted to make observations with both the Regular and Drifts cycles twice per month for periods of 24 hours. In 1969, this was reduced to one 24-hour operation of each type per month. Periods when these measurements were carried out are listed in Tables V and VI.

IV. ANALYSIS

A. Introduction

A computer program, which employs as input the digital data tape on which all the radar data are stored, has been written to analyze the results obtained in the Regular and Drifts observations. Early in the development of the new system, we planned to perform all data processing at the completion of each run, or cycle of runs, thereby eliminating any post-processing and providing the final results in usable form in real time. This still appears to be a desirable goal, but because the data collection and data analysis programs both grew in complexity, we decided to separate them, allowing data collection to commence prior to the availability of an entirely satisfactory analysis program.

The analysis program described here has been under development for some time and, although open to further refinement, is now probably close to final form. The program provides a smooth electron density profile that is corrected for the effects of the ratio of T_e/T_i on the electron scattering cross section, and yields electron temperatures T_e corrected for the effects of the variation of Debye length with altitude. As such, the density measurements depend upon the temperature measurements, and vice versa, so that an iterative processing scheme is required.

Table VII lists the data provided by the programs discussed in the previous section. As is evident from the table, the height resolution for the density measurements considerably exceeds

TABLE V

REGULAR UHF OBSERVATIONS PRIOR TO JANUARY 1970

Date	Start (GMT)	End (GMT)	Comments
1968			
15-16 August	1500	1400	
22-23 August	1800	1700	
29-30 August	1300	1300	
12-13 September	2000	2000	
19-20 September	1300	1300	
3-4 October	2030	2230	
22-23 October	1300	1300	
14-15 November	1530	1530	
25-26 November	1500	1500	
17-18 December	1400	1400	
30-31 December	1500	1530	
1969			
16-17 January	1430	1430	
5-6 February	1430	1400	
26-27 February	1530	1530	Antenna gain low owing to snow
21-22 March	2120	1010	
23-24 March	0140	1000	Aurora
9-10 April	1430	1430	
6-7 May	1300	1300	
5-6 June	1330	1400	
1-2 July	1300	1315	
14-15 August	1315	1345	
9-10 September	1415	1400	
30 September, 1 October	0300	1400	Aurora
3-4 November	1900	2200	
8-9 December	1745	1745	

TABLE VI

DRIFTS UHF OBSERVATIONS PRIOR TO JANUARY 1970

Date	Start (GMT)	End (GMT)	Comments
1968			
2-3 August	0100	0200	Na cammutatian
8-9 August	0230	1130	Na commutatian
13-14 August	1530	1530	Na cammutatian
20-21 August	1300	1400	
27-28 August	1330	1330	
2-3 September	1700	1700	
11-12 September	1800	1800	
26-27 September	1400	1400	
8-9 October	1600	1800	
29-30 October	1500	1500	
19 Navember	1700	2300	
29-30 Navember	1400	1400	
12-13 December	1700	1800	
1969			
31 January	0100	1300	
12-13 February	1420	1450	
25-26 March	2130	2130	
23-24 April	0320	0310	
30 May	1300	2200	Cammutating failed at 2200
1 June	0050	1200	Bad data tape priar ta 1 June
23-24 June	1320	1310	
9-10 July	1140	0945	
29-30 July	2300	2400	
26-27 August	2030	2030	
23-24 September	1300	1300	
14-15 October	2200	2200	
20-21 Navember	1330	1500	
22-23 December	2045	2045	

TABLE VII

DATA AVAILABLE FOR PROCESSING

Mode	Height Resolution (km)	Sample Spacing (Density) (km)	Heights for Temperature Measurements (km)
A	15	7.5	None
B	75	30	225, 300, 375, 450, 525, 600, 675
C	150	30	450, 525, 600, 675, 750, 825, 900, 975, 1050, 1125

that for the temperature measurements. Advantage is taken of this when constructing the density curve by using only the A-mode data up to an altitude above $h_{max}F2$.

B. Electron and Ion Temperatures

In essence, the electron and ion temperatures are obtained by comparing the observed spectra with those computed theoretically for different temperatures. These theoretical spectra were calculated using expressions published by Fejer,[10] and assume the following: the electrons and ions each have a Maxwellian velocity distribution, but need not be at the same temperature; all ions are singly charged; collisions with neutrals and the influence of the earth's magnetic field may be neglected. For the observations described here, we believe all these conditions have been met.[11] In carrying out the calculations, we also assume that O^+ is the only ion present. This assumption appears to be valid at Millstone, at least over most of the altitudes examined. For the measurements made at 225-km altitude, the pulse also illuminates regions beneath where O_2^+ and NO^+ are present – especially in summer.[12,13] Neglecting the presence of these ions in the reduction should cause both T_e and T_i to be slightly underestimated.

At high altitudes (>750 km), it is possible that small numbers of light ions (H^+, He^+) are present which will cause T_i to be overestimated. However, from the observed signal spectra, we have not yet been able to identify regions in which a significant abundance ($\gtrsim$25 percent) of H^+ or He^+ is present. A final assumption made in the calculations is that the plasma frequency is 10 MHz. This is equivalent to assuming that the Debye length D_e is very small and is justified only at altitudes below about 450 km. Once an estimate has been made of the Debye length, it is possible to correct for this assumption as discussed below.

The fluctuation spectrum W(f) of the plasma, calculated in the manner outlined above, is next convolved with the function [Eq. (4)] representing the instrumental resolution set by the pulse length T. With the computer program presently available, these calculations do not proceed quickly enough to permit a point-by-point comparison of the measured and theoretical spectra in a least-mean-squares sense. Instead, the reduction is carried out by comparing two parameters that characterize the spectra – namely, the ratio of the power in the wings to that at the center frequency, and the spectrum width (to a point of half-peak power). The ratio and width of the theoretical spectra were obtained, and polynomial expressions were then derived (by least-mean-squares fitting in a computer) to yield T_e and T_i as functions of these two parameters.

These functions each employ ten terms and allow the measured ratio and width to be converted to temperature to an accuracy of 1 percent or better. Different functions are required for each of the pulse lengths employed, and, in order to obtain sufficient accuracy, different equations are employed depending upon whether T_e/T_i is greater or less than 2.0.

To recover the ratio parameter for each measured spectrum, parabolas are fitted to the four center points and four points in the wing of the spectrum chosen to include the highest adjacent pair. Figures 5 and 6 are flow diagrams showing the procedure employed for fitting the two parabolas and ensuring that they are of correct shape. In order to locate the position in frequency of the half-peak value, linear interpolation is employed between the pair of points on the edge of the spectrum whose amplitudes bracket the half-peak power value.

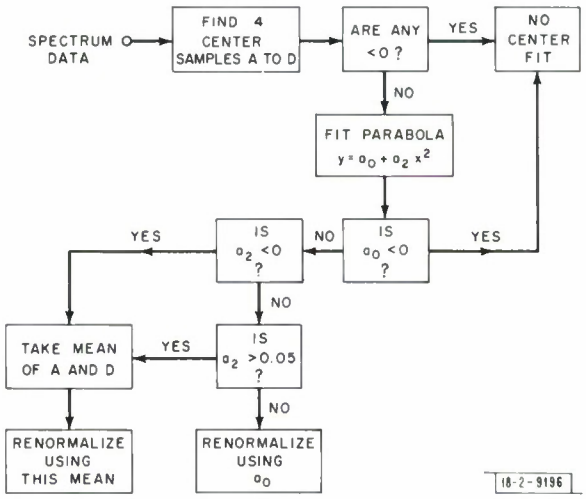

Fig. 5. Method of renormalizing by fitting a parabolo to center of spectrum.

When determining the ratio and width parameters, the two halves of the spectrum are analyzed separately, and independently converted to estimates of electron and ion temperatures. In addition, a mean is taken of the ratios and widths and is also used to obtain T_e and T_i. Because it should be insensitive to shifts in the spectrum introduced by drifts (Sec. IV-D), this mean value is adopted as the best estimate where both halves of the spectrum have been successfully analyzed.

Moorcroft[14] has shown that the effect of increasing the Debye length D_e on the spectrum shape is exactly equivalent to lowering the ratio T_e/T_i. Thus, spectra interpreted on the assumption that $D_e \to 0$ yield a fictitious value β for the electron-to-ion-temperature ratio that is related to the true value T_e/T_i in[14]

$$\frac{T_e}{T_i} = (1 + \alpha^2)\,\beta \qquad \alpha \leqslant 1 \tag{7}$$

where $\alpha = 4\pi D_e/\lambda$, and $D_e = (kT_e/4\pi Ne^2)^{1/2}$ in which N is the electron density and e is the electronic charge. Since the estimate of T_i does not depend upon α, this means that only the initial estimate T_e' of the electron temperature is in error.[14] For our wavelength, the correction formula reduces to

$$T_e = T_e' \left(1 - \frac{1.62\ T_e'}{N}\right)^{-1} . \tag{8}$$

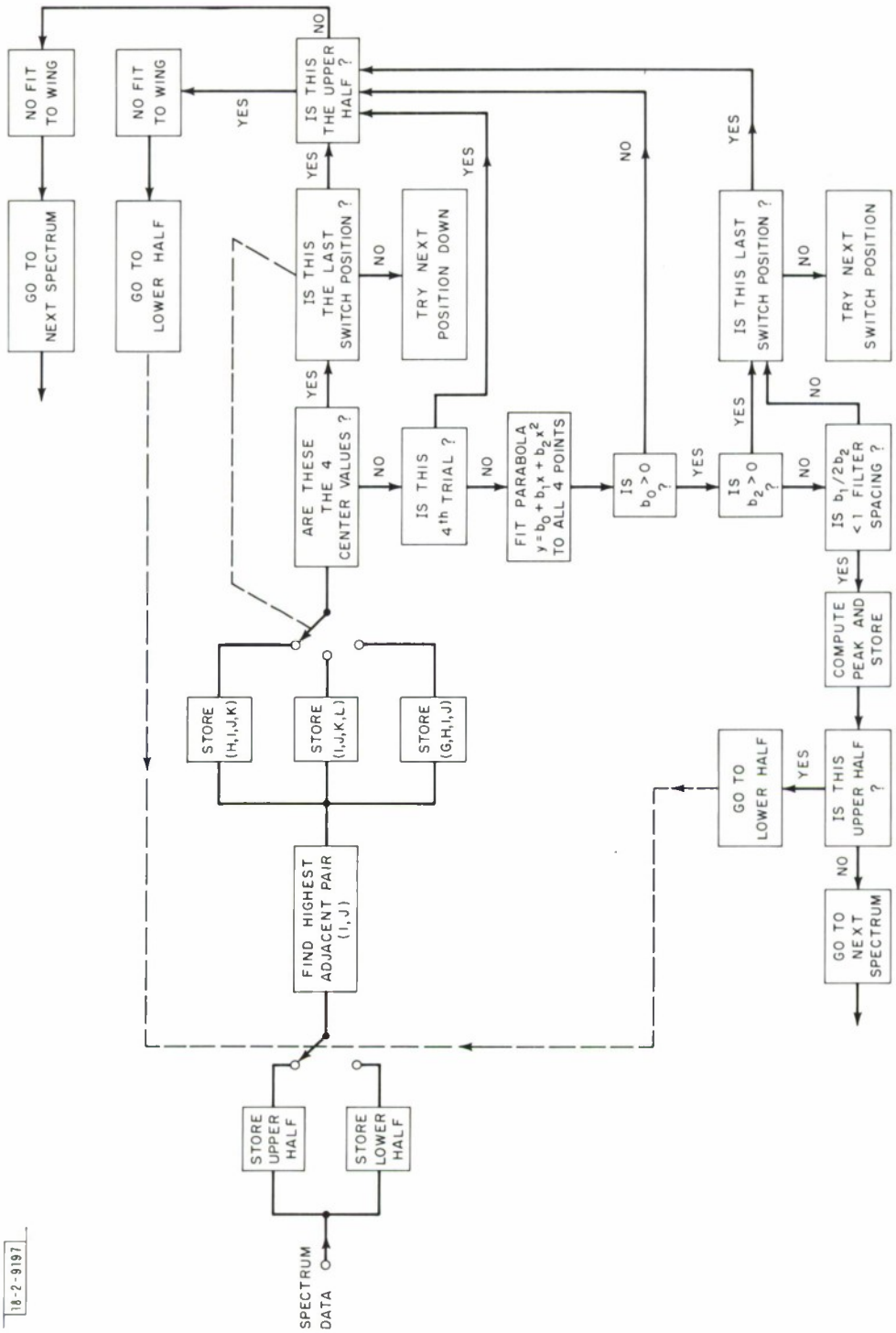

Fig. 6. Method of finding height of wing by fitting a parabola.

Evidently, to obtain the true temperature, it is necessary to know the density N. Thus, at this stage, reduction of the temperature data is halted until the density profile has been reduced. When this has been done, corrected values of T_e are obtained via Eq. (8). These are next employed in a recomputation of the density profile, and this revised estimate of N is then used to yield a second, more accurate estimate of T_e. We feel that the accuracy achieved this way is sufficient for all practical purposes, but, of course, further iterations could be performed.

C. Electron Density

The electron density-vs-altitude distribution is obtained by combining data obtained in the A-, B-, and C-mode runs to yield the shape of the profile, and by normalizing this to have the correct peak density set by

$$N_{max} = 1.24 \times 10^4 (f_oF2)^2 \qquad \text{electrons/cm}^3 \tag{9}$$

where f_oF2 is in megahertz. The value of the F-region critical frequency is measured and stored prior to each A-mode run (Sec. III-C), hence, all the information needed to process the results is available on the data tape. However, a new table of f_oF2 values may be substituted via punched cards.

The principal difficulty encountered in writing the present computer program was in devising a way of combining the A, B, and C results to obtain the shape of the profile. Previously, the parameter $\log_{10}\sigma_r$ [Eq. (6)] was machine plotted, and a single curve was obtained by overlaying these curves for the best fit. That is, the A-mode results, which provide the best height resolution, were allowed to control the results up to some point above h_{max} where they became noisy. A smooth transition was then made to the B-mode results, and at some higher altitude to the C data. This combined curve was then corrected for the effect on the scattering cross section of T_e/T_i (Ref. 1).

When attempting to obtain a computer program to perform these tasks, we encountered considerable difficulty in devising a method that yielded a smooth profile. Typically, changes in the density gradient would be encountered whenever there was a transition from the data obtained in one mode to another. In the method finally adopted, the data are renormalized so that in certain altitude ranges common to two modes the points have a common center of gravity. A single curve through all the points is then obtained by least-mean-squares, each point being weighted in proportion to its signal-to-noise ratio.

The program proceeds by treating all the data obtained between successive A-mode runs as a set. Where more than one run (B, C, or D) of the same kind has been made (as in the Drifts program) the values of the echo power T_r are summed and divided by $\sqrt{nq}$, where n is the number of runs of the same type, and q is the ratio of their length to the length of the A-mode run. This serves to normalize the results so that the relative uncertainty in each point is inversely proportional to its absolute value.

Owing to the fact that the density falls by about two orders of magnitude in the region between h_{max} and 1000 km, it becomes difficult to employ a least-mean-squares curve-fitting procedure, since the shape of the curve will be dominated by the large values of density at low altitudes. For this reason and because the density decreases exponentially, or very nearly so, it is convenient to work with the logarithm of the density. Thus, the logarithm is taken of all the values of T_r obtained in each run over the height range for which $T_r \geq 0$. Next, the effects of height h

and temperature ratio on the results are removed by computing

$$\log_{10} N = g(h) + \text{const} \tag{10}$$

where

$$g(h) = \log_{10}(T_r) + 2 \log_{10}(h) + \log_{10}(1 + \beta) \tag{11}$$

and β is the initial estimate of T_e/T_i [Eq. (7)].

To obtain the height dependence of β required in Eq. (11), the following scheme is employed. For $h \leqslant 225$ km, linear interpolation between the value observed at 225 km and an assumed value $\beta = 1.0$ at 130 km (Ref. 12) is employed. Between 225 and 600 km, all the available values of β at each altitude (Table VII) are averaged and $\beta(h)$ again obtained by linear interpolation between each pair of points. A straight line is fitted by least-mean-squares to all the values obtained in the C-mode for $h \geqslant 600$ km and employed at these altitudes for the height dependence of β, provided that $\beta \rightarrow 1.0$ as $h \rightarrow \infty$. In the event that the slope of the fitted straight line is positive, linear interpolation is used between the observed mean value at 600 km and an assumed value $\beta = 1.0$ at 1500 km. These procedures serve to ensure that the third term in Eq. (11) is well behaved. The discontinuities in the gradient $d\beta/dh$ that are introduced cause only minor changes in the density curve; these are largely removed by the subsequent smoothing.

The next step is to renormalize the g(h) values for the A, B, and C data so that, for certain common altitude regions above h_{max}, they have the same centers of gravity. To do this, use is made of the fact that dg(h)/dh is nearly constant. Thus, a curve of second order is fitted to the g(h) results for the A-mode data above $h_{max} + 60$ km. A similar curve is fitted to the B-mode data above $h_{max} + 200$ km. A shift is then made to the B-mode curve to cause it to intersect the A-mode curve at the midpoint of the height interval common to the two sets of data. The C-mode results are normalized to the B-mode results in a similar fashion.

In fitting these second-order functions to the data, an attempt is made to remove spurious points caused, for example, by echoes from satellites that occasionally pass through the beam. Thus, when the curve is first fitted each point is weighted inversely as the square of its height. Next, all points that deviate from the curve by more than five standard deviations are removed, and the curve refitted to the remaining points. In the second fit, each point is weighted by the original value of temperature T_r. (Although the relative uncertainty in the points is proportional to T_r^{-1}, the temperature cannot be used to weight the points until spuriously large ones have been removed.)

With the three sets of points thus normalized, a new second-order function is fitted to all the points between $h_{max} + 60$ km and the highest point available, each point being weighted according to its value. This curve is taken as the variation of g(h) above $h_{max} + 100$ km, and below this altitude the unsmoothed A-mode data are employed. The constant term in Eq. (10) is determined by fitting a parabola to the points in the vicinity of the peak and renormalizing so that $N = N_{max}$ [Eq. (9)] at h_{max}.

These steps yield an initial estimate of the density variation that is employed to correct the electron temperature results via Eq. (8). As discussed above, this yields revised values of the ratio T_e/T_i permitting a new estimate of g(h) from

$$g(h) = \log_{10} T_r + 2 \log_{10} h + \log_{10}[1 + (T_e/T_i)] \quad . \tag{12}$$

The variation of T_e/T_i with altitude is obtained in exactly the same way as the variation of the initial estimate β. The curve fitting, renormalization, and final smoothing are then all performed again, exactly in the same manner, to yield the final density curve.

D. Vertical Drift Velocity

If the ionospheric plasma in the scattering volume sampled by the radar has a mean radial velocity v_d with respect to the radar, the entire spectrum will be shifted by an amount

$$\Delta f_d = \frac{-2v_d}{\lambda} \qquad \text{Hz} \quad . \tag{13}$$

For the Millstone Hill radar (λ = 68 cm), this corresponds to

$$\Delta f_d \sim -3v_d \qquad \text{Hz} \tag{14}$$

when v_d is in meters/second.

Since the vertical drifts in the ionosphere are at most a few tens of meters per second, Δf_d is typically less than 100 Hz. The overall width of the spectrum on the other hand usually exceeds 10 kHz, thus, extremely precise spectrum measurements are required if the presence of a drift of the plasma is to be detected. Despite this, the results of the C-mode observations clearly reveal effects due to drifts. Various methods of extracting the drift information have been tried and compared, and the results have been published elsewhere.[15] Here, we shall simply summarize the approach that was finally taken.

Woodman and Hagfors[7] have discussed in detail the method and accuracy of the velocity determination procedure adopted at Jicamarca. In this scheme, the average phase shift $\Delta\varphi$ between a pair of short transmitted pulses separated by τ seconds is obtained. Since the phase shift $\Delta\varphi$ is determined by

$$\Delta\varphi = 2\pi\Delta f_d \tau \qquad \text{radians} \tag{15}$$

it is possible to recover the drift velocity. The accuracy of measurement initially improves with increasing the pulse separation τ, but subsequently falls because the pulses become uncorrelated. Thus, Woodman and Hagfors[7] give for the rms velocity uncertainty

$$\Delta v_d = \frac{1}{(2n)^{1/2}} \frac{\lambda}{4\pi} \frac{[1 - S(\tau)^2]^{1/2}}{\tau S(\tau)} \qquad \text{m/sec} \tag{16}$$

where n is the number of pulse pairs transmitted, and $S(\tau)$ is the normalized echo amplitude correlation for pulses spaced τ sec apart.

The great advantage of the complex correlation function approach is that (for symmetrical spectra) the phase of the function contains all (and only) the information concerning the doppler shift, while the shape is defined separately by the normalized echo amplitude correlation function $S(\tau)$. These advantages can be achieved for the Millstone Hill data by taking the complex Fourier transform of the measured power spectrum. A set of real $a(\tau)$ and imaginary $b(\tau)$ parts are then obtained where

$$\tau = 0, 1, \ldots, 11(NF)^{-1} \qquad \text{sec}$$

in which N is the number of points in the original spectrum (24), and F is their spacing (1 kHz). The phase shift $\Delta\varphi_\tau$ at each of these spacings is simply

$$\Delta\varphi_\tau = \tan^{-1}\frac{b(\tau)}{a(\tau)} \quad . \tag{17}$$

In order to use all the possible estimates of $\Delta\varphi_\tau$, two different approaches have been tried. In the first, a least-mean-squares straight line was fitted to the $\Delta\varphi_\tau$ results. However, only the first 6 of the 12 points were considered significant, and each of these was first weighted according to the square of the amplitude correlation at that spacing, i.e., an amount

$$c^2(\tau) = a^2(\tau) + b^2(\tau) \quad . \tag{18}$$

The slope α of this least-mean-squares straight line was taken to be the rate of change of phase with spacing $\Delta\varphi/\tau$ and employed in Eq. (15) to determine v_d.

The least-mean-squares approach was later recognized to be "suboptimum," since points at large spacings τ tend to control the slope α. It may be shown that the optimum procedure is to search for the value of α that maximizes the sum[15]

$$I = \left| \sum_\tau [a(\tau) + jb(\tau)]\, S(\tau)\, e^{-j\alpha\tau} \right| \tag{19}$$

in which $a(\tau)$ and $b(\tau)$ are the real and imaginary parts of the transformed measured power spectrum, $S(\tau)$ is the expected correlation (root sum square of real and imaginary parts) at each spacing, and α is the unknown slope of the phase function, i.e., $\Delta\varphi/\tau$. This process amounts to multiplying each vector (a + jb) by a second vector and summing. In this way, each vector is weighted by its expected length, and the vectors are progressively rotated until the largest vector sum I is obtained. This occurs when each second vector is the complex conjugate of the first.

The weight function $S(\tau)$ depends only upon the shape of the spectrum and hence can be obtained from the experimental observations. In the case of the Millstone Hill data, a mean of the correlation functions $c(\tau)$ obtained in four successive 8-minute runs is taken as the weight function employed in Eq. (19). As a trial value of α, the value obtained from the least-mean-squares fit to the phase data (above) is first employed. The sum I is then recalculated for values of α differing by ±5, ±10, and ±15 percent. Finally, a parabola is fitted to the seven values of $I(\alpha)$ and the peak of this parabola taken as the best estimate of α. In the event that the peak of the parabola lies outside the range ±15 percent of the initial value, only the least-mean-squares estimate of the drift is accepted.

In practice, the optimum and least-mean-squares straight-line procedures are found to yield almost identical results, so that the additional calculations to compute the optimum estimate of α may be unwarranted. Thus, a shorter version of the program to extract the drift information has been written that employs only the least-mean-squares approach. This version has been incorporated into the program that analyzes the density and temperature results as described above.

V. RESULTS

A. Electron Density

The final electron density profile is made available on a high-speed printout in the form of $\log_{10} N$ as a function of altitude. For altitudes between 100 km and h_{max} + 100 km, the A-mode results (which yield a point every 7.5 km) are employed without any smoothing. At higher altitudes, the smooth curve fitted to the combined A-, B-, and C-mode data is used. Points are

tabulated every 10 km up to 600 km, and subsequently every 25 km up to 1000-km altitude. Any results obtained for the region above 1000 km are tabulated at 50-km intervals. All these data are also written on a "plotting" tape and a master data tape. The plotting tape is used to drive a CalComp plotting machine to yield plots of the logarithm of the density over the height range 100 to 1100 km. The density scale runs from 10^3 to 10^7 electrons/cm^3. Figures 7(a-f) provide examples of plots produced in this way.

The master data tape is employed to accumulate results made over a long period of time, so that it should eventually be possible to search for seasonal variations and perform other examinations of the data that depend upon having a statistically large sample.

In Figs. 7(a-f), the presence of ground-clutter echoes (Sec. II-B) at ranges near 150 km has given rise to spurious density values between 130 and 160 km. For the daytime measurements, it is possible to extrapolate through this interval using as a guide the measurments near 120 km. Below this altitude, the measurements are again suspected owing to the presence of further clutter echoes near 100 km; these are clearly evident at night.

In some instances, the second-order function fitted to the results above h_{max} does not decrease monotonically with altitude. This could result from the presence of spurious points caused by satellite echoes that were not removed from the data. In these cases, the computation of the density is made to halt when the gradient dN/dh becomes positive. In Figs. 7(d-f), the density plot is not carried all the way to 1100 km for a different reason; namely, in order to indicate the quality of the results, the curve is halted at the altitude at which the uppermost valid data point was obtained.

The absolute accuracy of the density determination depends to a large extent on the reliability with which f_oF2 has been determined. For this reason, we plan to carry out the analysis of most of the data employing the option of substituting new values of f_oF2 (on punched cards) for those recorded in real time. These values can be obtained by plotting f_oF2 obtained from the ionosonde film together with values obtained at nearby stations, viz., Billerica, Massachusetts (42.6°N, 71.3°W), Ottawa, Canada (45.4°N, 75.9°W), and Wallops Island, Virginia (37.9°N, 75.5°W). A smooth curve is then drawn to follow the Millstone values except where an obvious misinterpretation has been made. This procedure probably provides f_oF2 accurate to 0.2 MHz, so that at night the error in the densities might reach 15 percent from this source alone. Errors in the shape of the density profile stemming from the scatter of the points can be examined by comparing successive profiles. For the most part, these appear to be small, although in some cases a difference that increases with altitude is noted between successive profiles. At 1000-km altitude, these random errors are thought to be of comparable magnitude to the uncertainty in the absolute value of N_{max}. Thus, at night it is possible that the uncertainty in the density at 1000 km becomes as large as 20 percent.

B. Electron and Ion Temperatures

The electron and ion temperatures obtained for each spectrum are tabulated on the high-speed printout as a function of the delay of the spectrum. These same data are written on the plotting tape and the master data tape.

When plotting the spectrum results, different symbols are employed to distinguish the 0.5- and 1.0-msec results. A point is also added at 120 km equal to the fixed temperature (355°K) assumed in CIRA 1965 models. This serves to guide the eye over the interval below 225 km. The scale for the temperature plot is chosen from a binary series (1000°, 2000°, 4000°, 8000°K) in

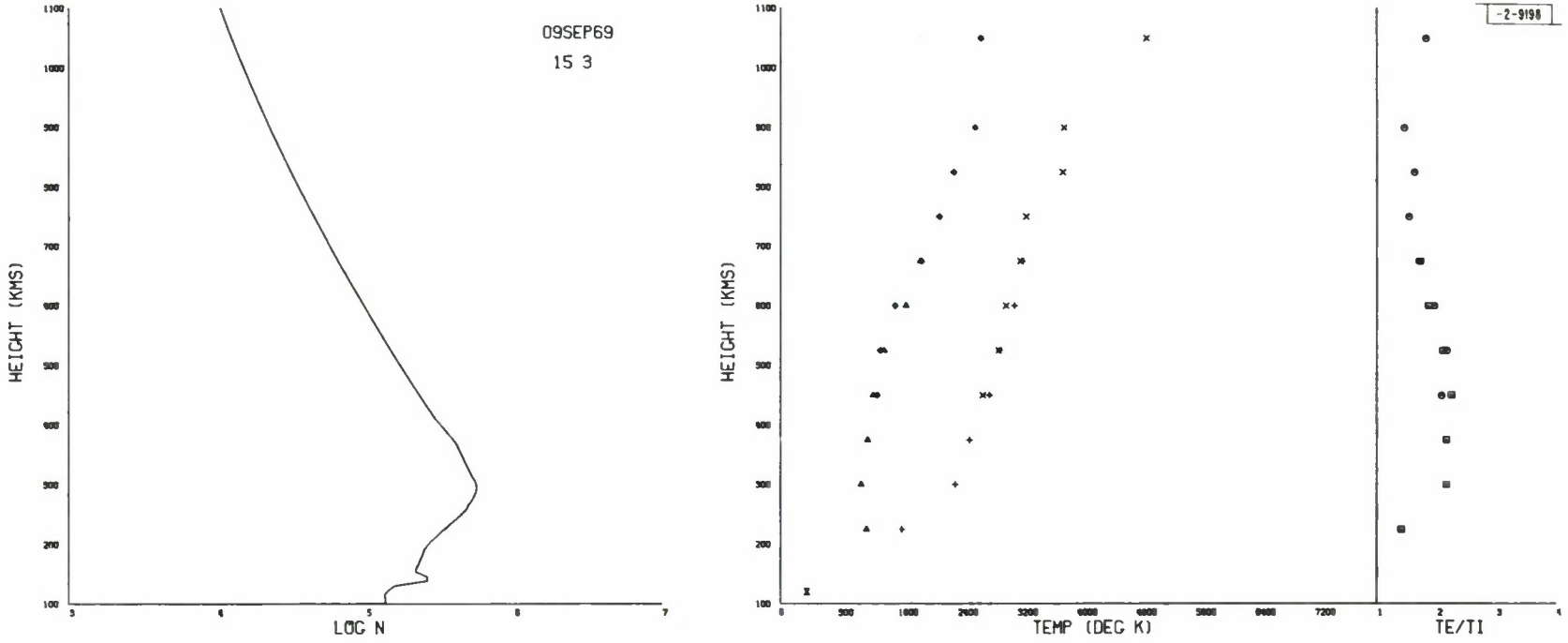

(a) 1503 GMT.

Fig. 7(a-f). Electron density (solid curve), electron temperature (crosses), and ion temperature (triangles and diamonds) obtained with new system during 24-hour observing period on 9-10 September 1969.

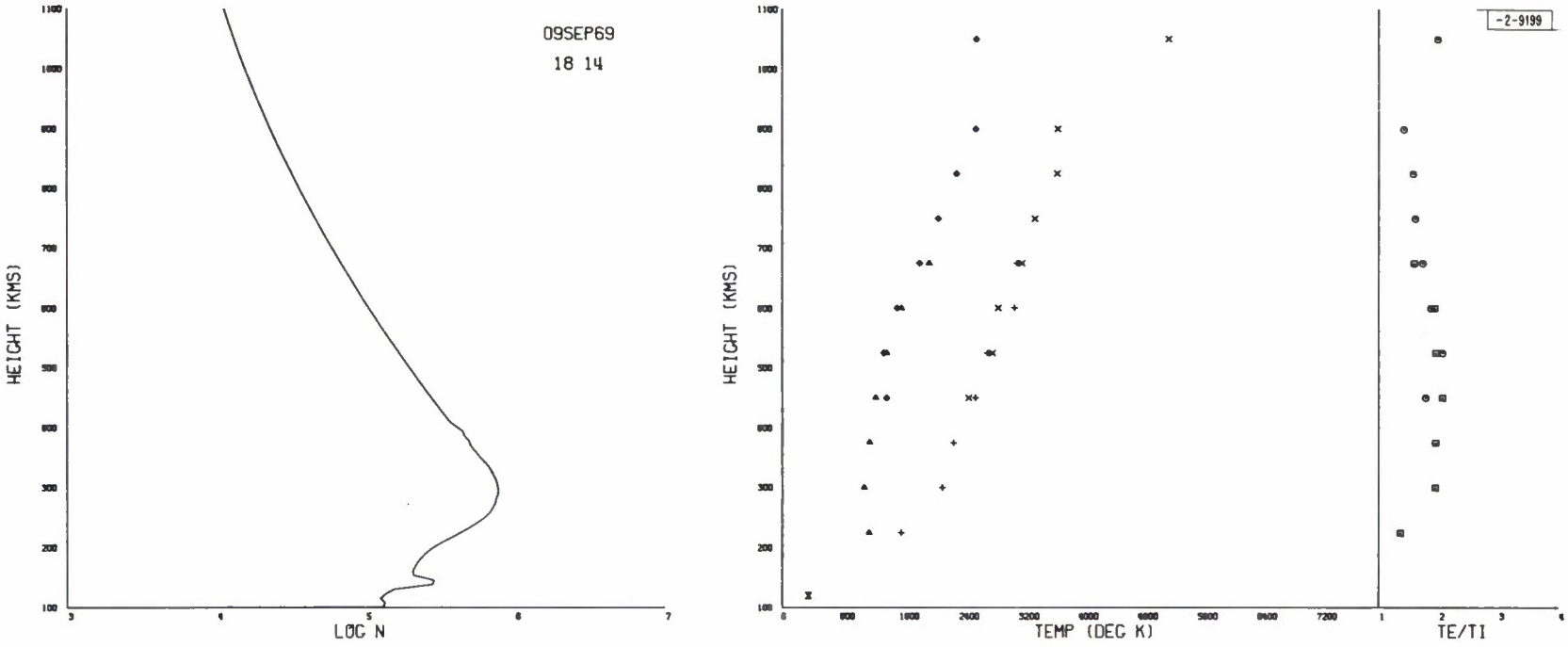

(b) 1814 GMT.

Fig. 7(a-f). Continued.

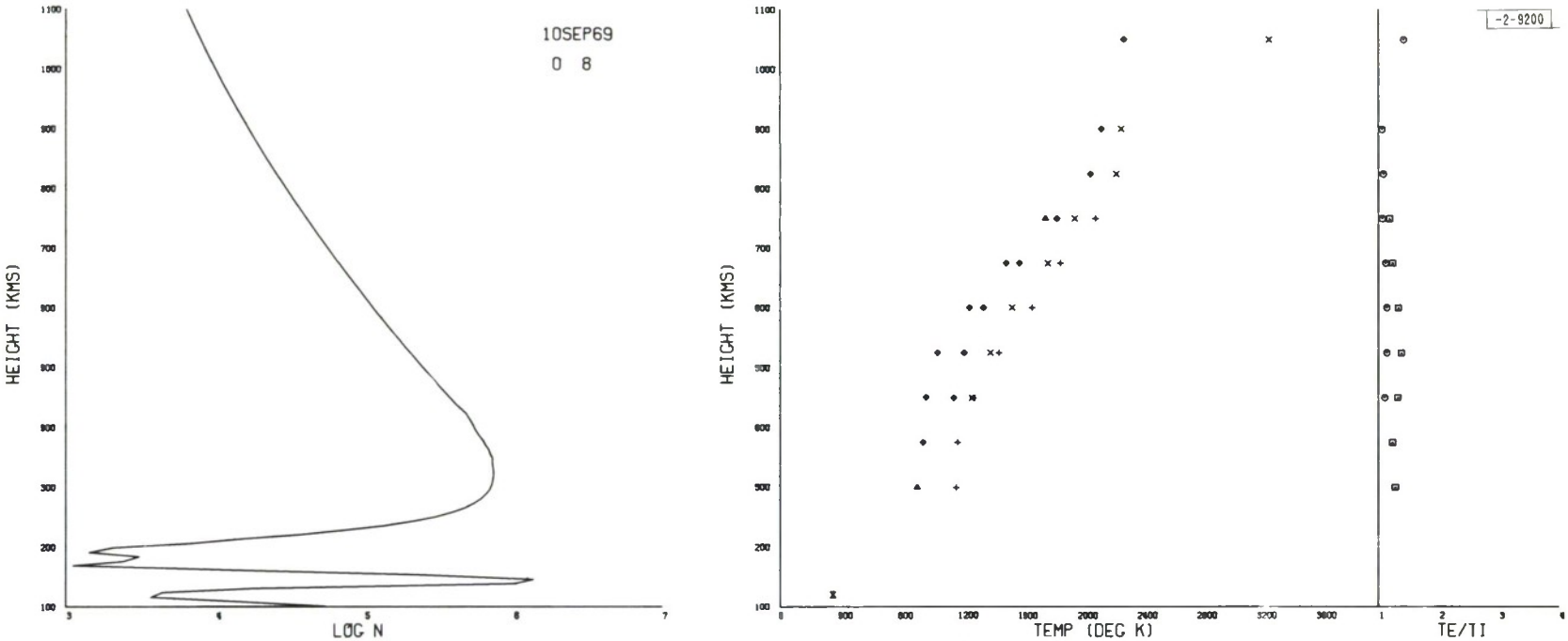

(c) 0008 GMT.

Fig. 7(a-f). Continued.

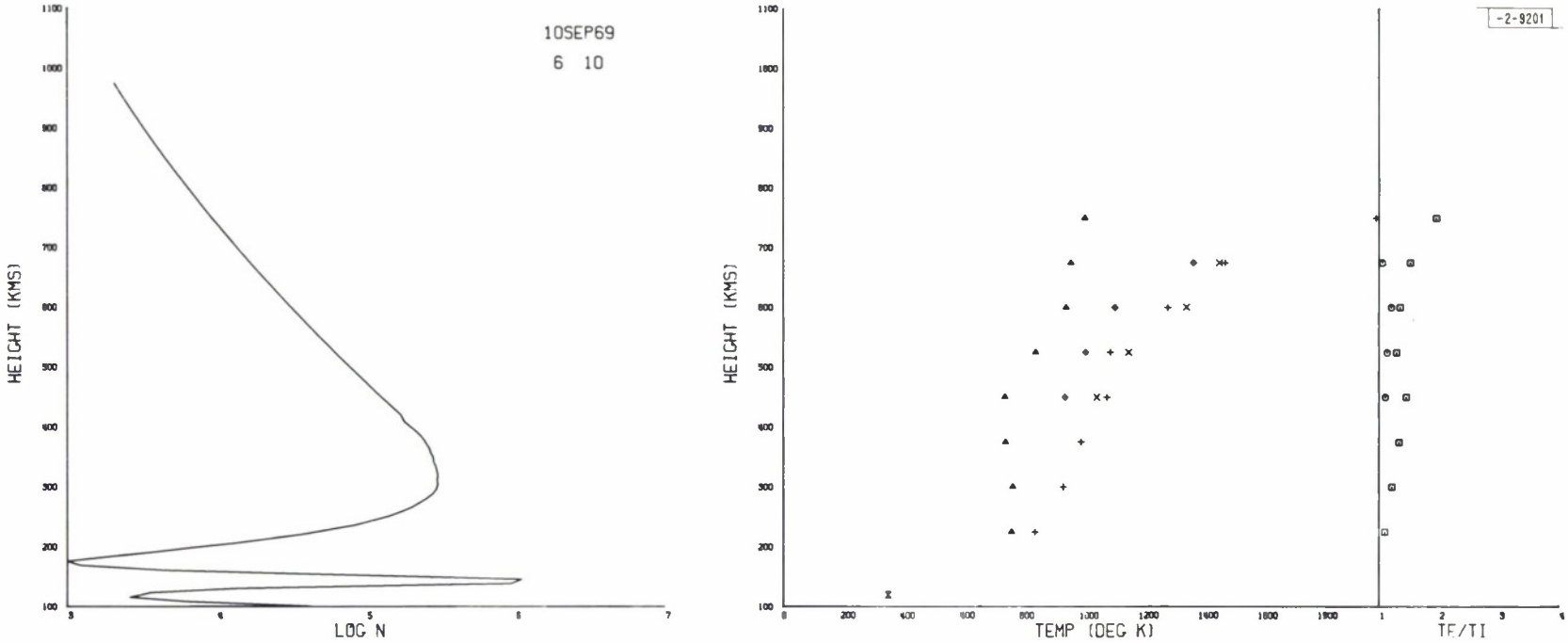

(d) 0610 GMT.

Fig. 7(a-f). Continued.

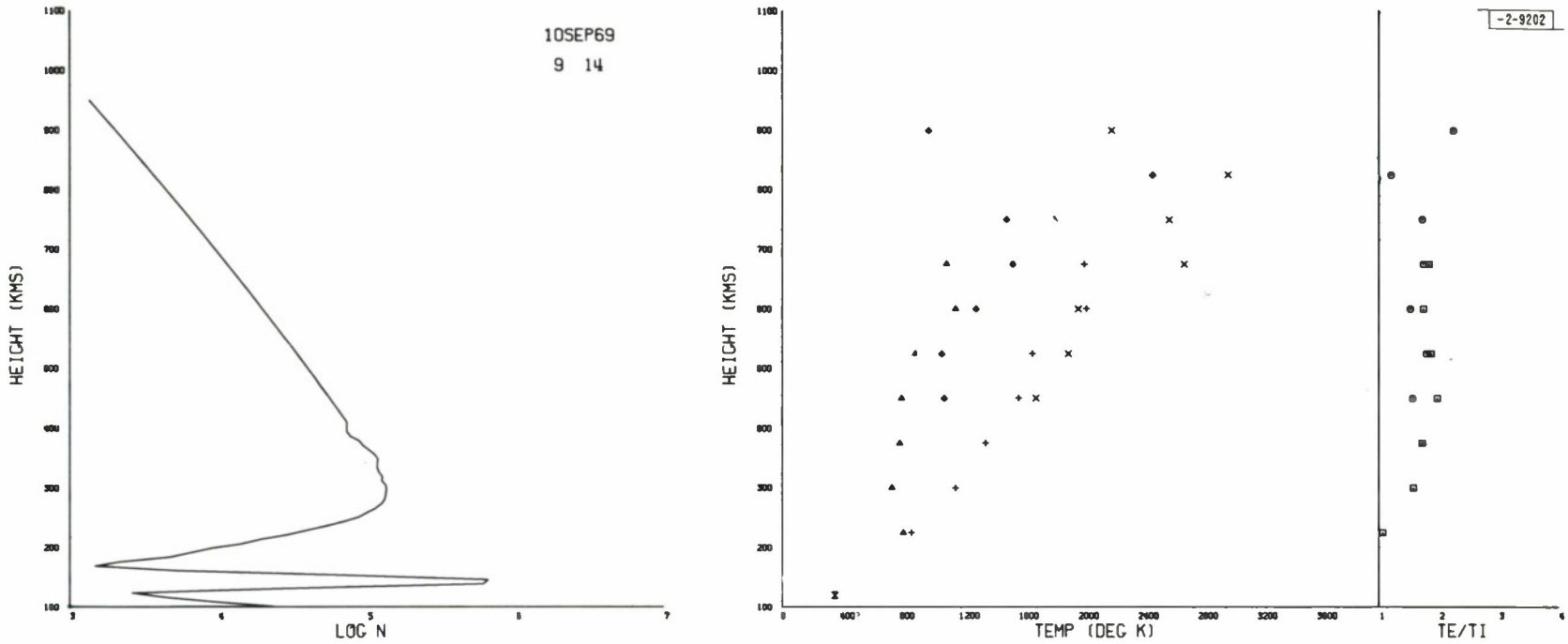

(e) 0914 GMT.

Fig. 7(a-f). Continued.

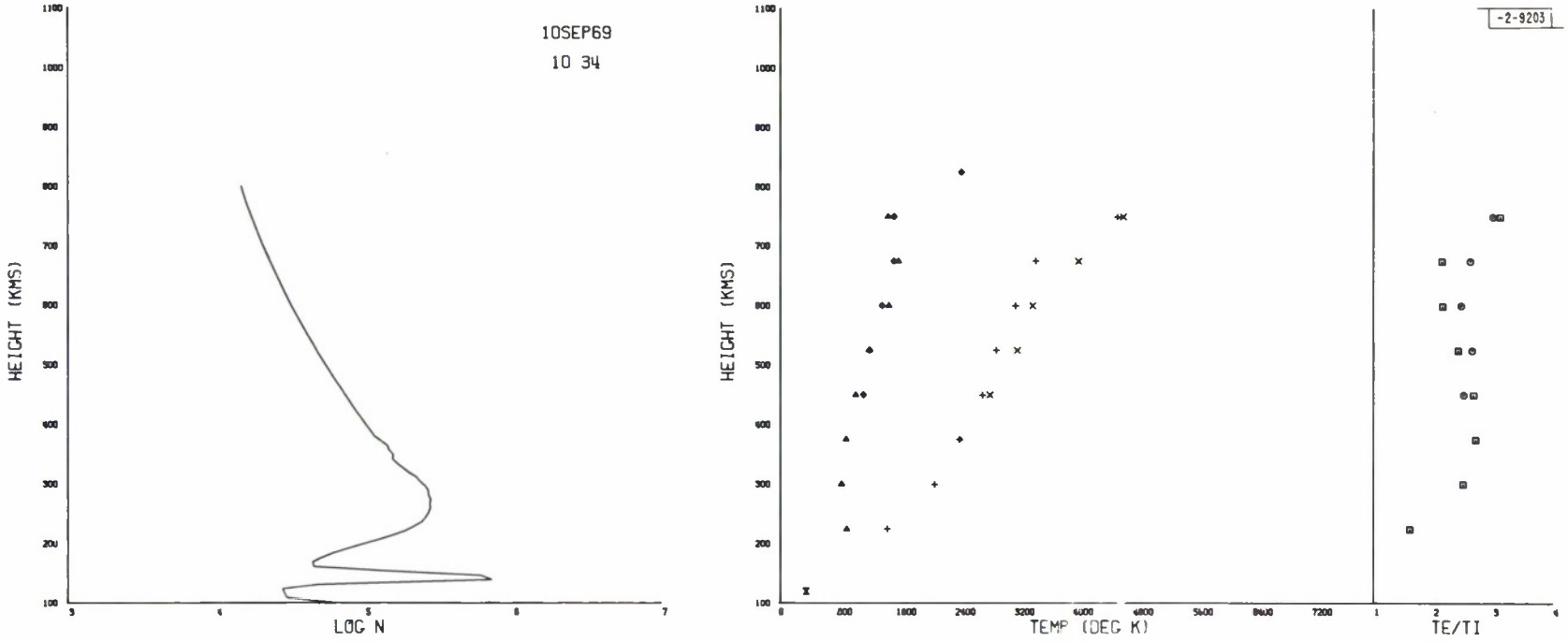

(f) 1034 GMT.

Fig. 7(a-f). Continued.

order to be able to accommodate the highest value available for the plot. The temperature ratio (T_e/T_i) results are also plotted on a fixed scale running from 1.0 to 4.0. Figures 7(a-f) provide examples of the temperature variation observed at various parts of the day for the observations made on 9-10 September 1969.

A number of features of these data deserve comment. Above ~500 km, the electron temperature should chiefly be governed by conduction of heat from the protonosphere. Thus, the temperature would be expected to increase smoothly with a slope $dT_e/dh \propto T_e^{-5/2}$. Up to an altitude of 900 km, most of the measurements exhibit this behavior, but T_e appears to increase in an unexpected fashion at higher altitudes. In order to reduce the experimental uncertainty, we have plotted in Figs. 7(a-f) only the average of the temperatures available for 975, 1050, and 1125 km. Despite this, a systematic deviation is usually observed. We have not yet determined the exact cause of this phenomenon, but believe that it could stem from the fact that Eq. (8) may over-correct the temperature values as $\alpha \rightarrow 1.0$ [Eq. (7)]. In order to circumvent this difficulty, corrections to the temperature results are not made if $\alpha^2 \geqslant 0.5$, and all such points are then discarded. Thus, we would not expect Eq. (8) to introduce a large error. The effect of an increasing abundance of light ions should be to increase T_i and possibly lower T_e/T_i, but this does not seem to be what is occurring. It suffices to say that this is one aspect of the reduction that warrants further investigation.

A second unsatisfactory feature of the temperature results is that at night there is a systematic difference between the values for T_i derived in the B- and C-modes. This is largely caused by different estimates of T_e/T_i for the two pulse lengths. In the daytime, on the other hand, the results agree remarkably well. This suggests that the difference is not caused by instrumental effects, but is introduced in the data analysis. The source of the discrepancy may be the equations employed to derive T_e and T_i from the parameters (width and ratio) of the spectrum. These equations may be inaccurate if the responses of the filters differ substantially from Eq. (2). The error introduced might be expected to be largest at night when the width of the spectrum is least. This point deserves further attention.

At present, the accuracy of the temperature values seems limited by these two systematic effects. During the daytime at altitudes in the range 225 to 600 km, the scatter in the temperature measurements seems to be 5 percent or less, suggesting that the random errors of measurement are small.

C. Vertical Velocity

Results for the vertical velocity obtained from the Drifts program are tabulated by the high-speed line printer as a function of delay, and are written on a plotting tape. These data are then usually plotted as a function of local time. Both the least-mean-squares and optimum estimates (Sec. IV-D) can be plotted. Figures 8(a-c) provide examples of the drifts observed at three altitudes during the measurements made on 25-26 March 1969.

The accuracy of the velocity measurements has been examined in detail.[15] It appears that the uncertainty increases with altitude, being ~±4 m/sec at 450 km and ~±10 m/sec at 900 km during the day, and ±6 to ±25 m/sec over this range at night. These uncertainties are set almost entirely by the signal-to-noise ratio achieved in the measurements, and do not depend greatly on the variation with time of the spectrum width or shape.

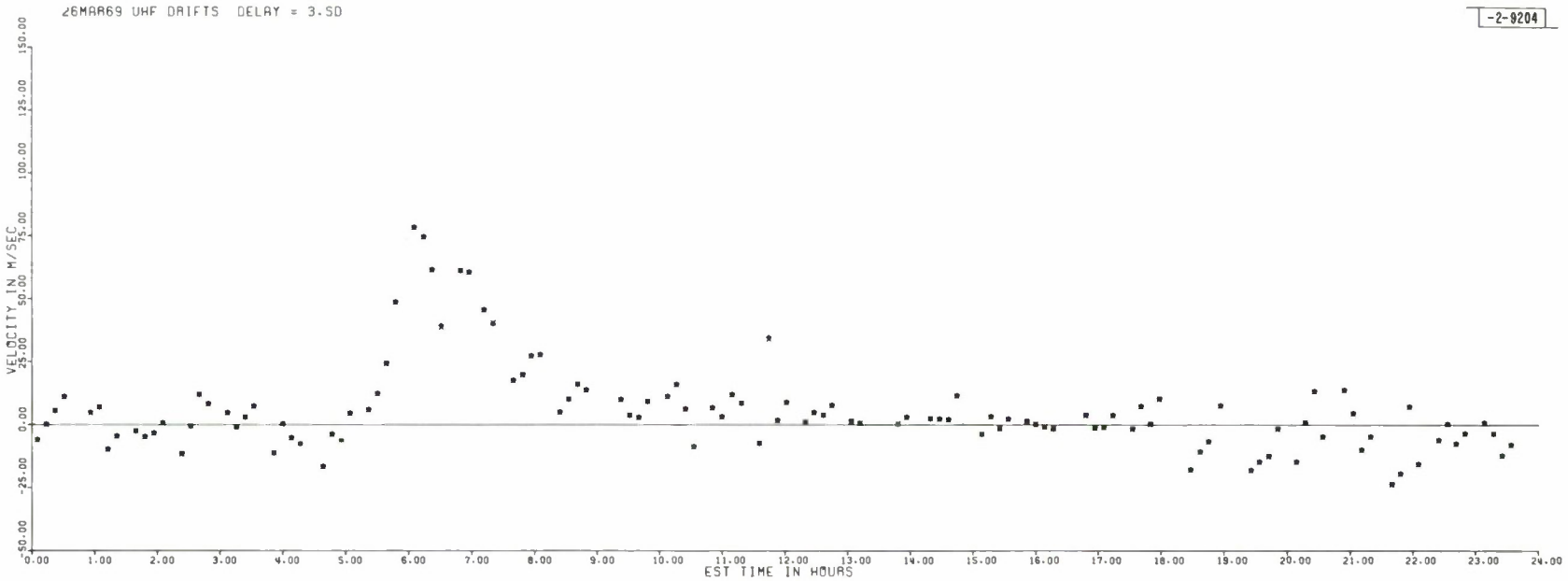

(a) At 525-km altitude.

Fig. 8(a-c). Vertical velocity derived from spectrum measurements during 24-hour observing period on 25-26 March 1969. Crosses represent values obtained by least-mean-squares method, and diamonds those from optimum method (Sec. IV-D).

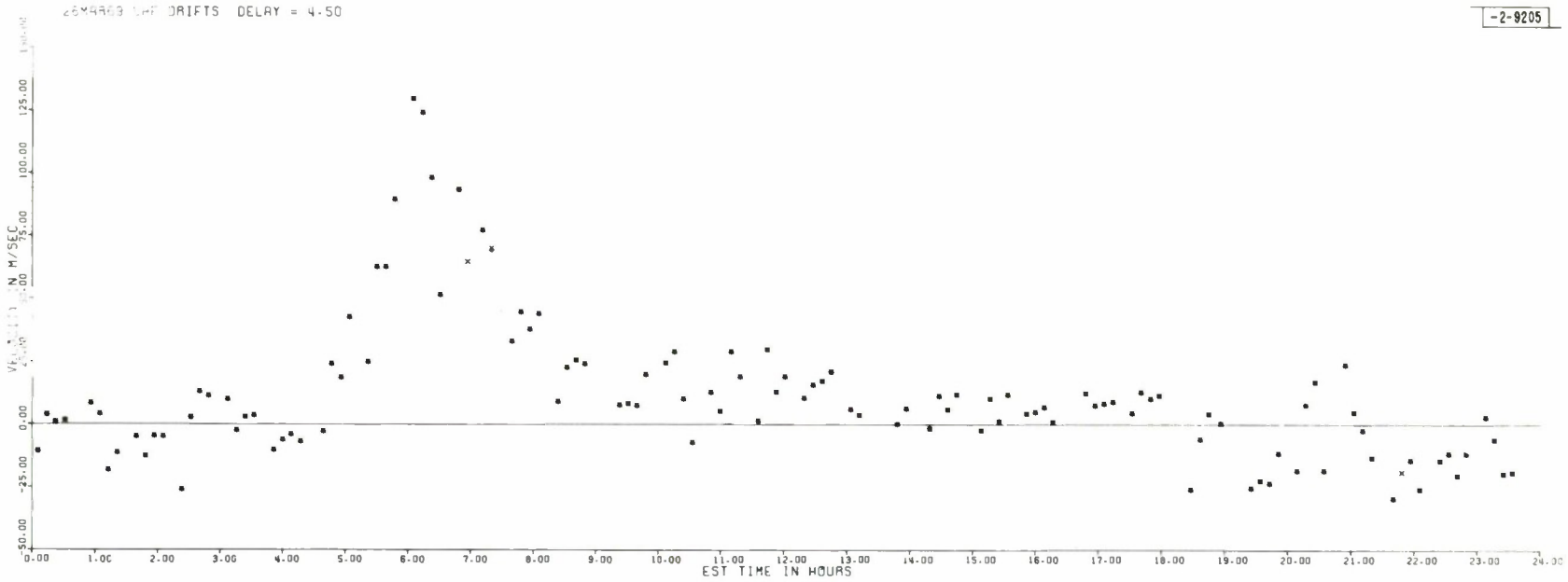

(b) At 675-km altitude.

Fig. 8(a-c). Continued.

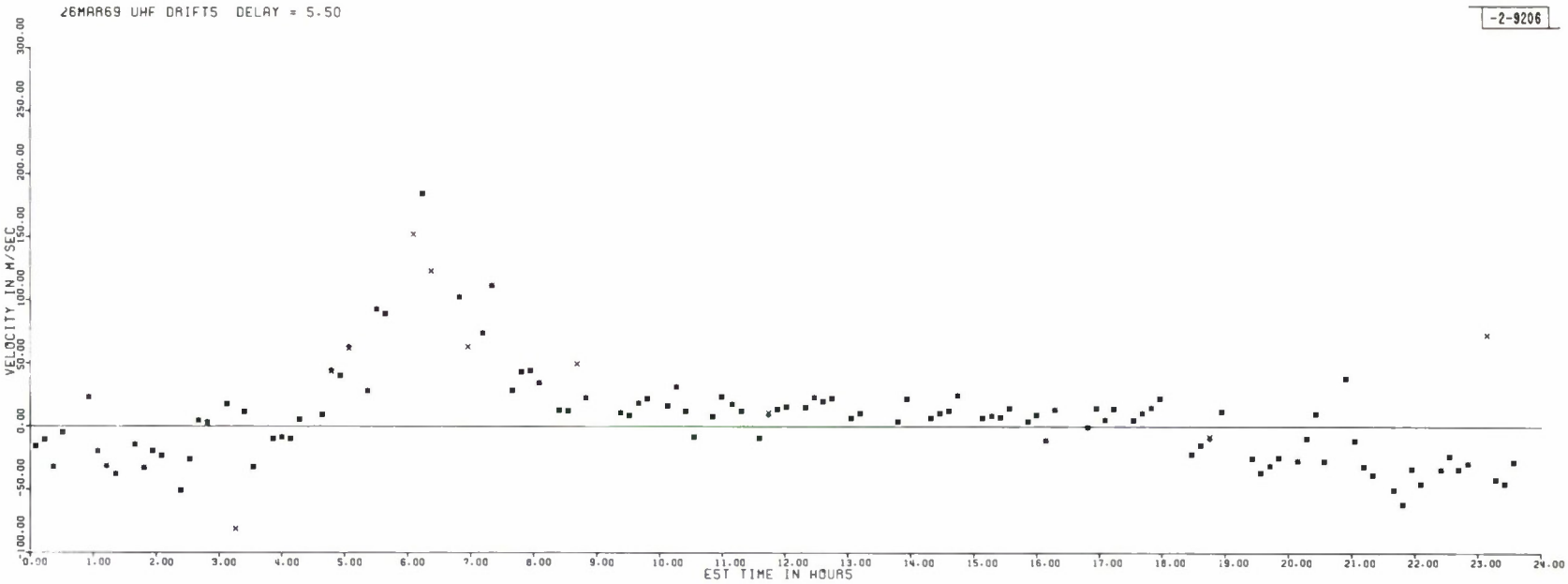

(c) At 825-km altitude.

Fig. 8(a-c). Continued.

ACKNOWLEDGMENTS

The authors wish to acknowledge the assistance of a number of colleagues in constructing the equipment described in this report, especially L.B. Hanson, J.H. McNally and A.H. Beauregard. We would like to thank others who contributed to the development of the computer programs, particularly J.K. Upham (Wolf Corporation) who wrote the section that treats the analysis of the density measurements, and R.A. Brockelman who wrote the program to analyze the drifts. Valuable suggestions concerning the data processing were made by L.A. Carpenter (University of Illinois) and R. Price (Sperry-Rand Corporation). We are also indebted to P.B. Sebring, under whose leadership the work was carried out.

REFERENCES

1. J.V. Evans and M. Loewenthal, Planet. Space Sci. 12, 915 (1964).
2. J.V. Evans, Planet. Space Sci. 13, 1031 (1965), DDC AD-616607.
3. _____, J. Geophys. Res. 70, 1175 (1965), DDC AD-614310.
4. _____, Planet. Space Sci. 15, 1387 (1967).
5. _____, Planet. Space Sci. (in preparation).
6. F. Perkins and R. Wand, "Analysis of the Ionosphere Incoherent Scatter Signal by Digital Methods," Report CRSR 207, Center for Radiophysics and Space Research, Cornell University (1965).
7. D.T. Farley, Radio Sci. 4, 935 (1969).
8. R.F. Woodman and T. Hagfors, J. Geophys. Res. 74, 1205 (1969).
9. J.W. Cooley and J.W. Tukey, Math. Comp. 19, 297 (1965).
10. J.A. Fejer, Can. J. Phys. 38, 1114 (1960).
11. J.V. Evans, Proc. IEEE 57, 496 (1969), DDC AD-694192.
12. _____, J. Geophys. Res. 72, 3343 (1967), DDC AD-658912.
13. J.V. Evans and L.P. Cox, J. Geophys. Res. 75, 159 (1970).
14. D.R. Moorcroft, J. Geophys. Res. 68, 4870 (1963).
15. J.V. Evans, R.A. Brockelman, R.F. Julian, W.A. Reid and L.A. Carpenter, Radio Sci. 5, 27 (1970).

DOCUMENT CONTROL DATA – R&D

(Security classification of title, body of abstract and indexing annotation must be entered when the overall report is classified)

1. ORIGINATING ACTIVITY *(Corporate author)* Lincoln Laboratory, M. I. T.	2a. REPORT SECURITY CLASSIFICATION Unclassified 2b. GROUP None

3. REPORT TITLE

Incoherent Scatter Measurements of F-Region Density, Temperatures, and Vertical Velocity at Millstone Hill

4. DESCRIPTIVE NOTES *(Type of report and inclusive dates)*

Technical Report

5. AUTHOR(S) *(Last name, first name, initial)*

Evans, John V., Julian, Ralph F., and Reid, Wallace A.

6. REPORT DATE	7a. TOTAL NO. OF PAGES	7b. NO. OF REFS
6 February 1970	44	18

8a. CONTRACT OR GRANT NO. AF 19(628)-5167 b. PROJECT NO. 7X263304D215 c. d.	9a. ORIGINATOR'S REPORT NUMBER(S) Technical Report 477 9b. OTHER REPORT NO(S) *(Any other numbers that may be assigned this report)* ESD-TR-70-98

10. AVAILABILITY/LIMITATION NOTICES

This document has been approved for public release and sale; its distribution is unlimited.

11. SUPPLEMENTARY NOTES	12. SPONSORING MILITARY ACTIVITY
None	Office of the Chief of Research and Development, Department of the Army

13. ABSTRACT

The Millstone Hill Thomson (incoherent) scatter radar system has been operated routinely since 1963 to perform a synoptic study of F-region electron densities, and electron and ion temperatures. This report describes system changes made in 1968 which considerably increased the accuracy of the measurements and allowed their extension to higher altitudes. These changes have also made it possible to measure the vertical velocity of the plasma over the altitude range 450 to 900 km to an accuracy on the order of 5 to 10 m/sec, depending upon altitude and time of day.

Of even greater significance, complete machine reduction of the results is now possible so that considerable savings in time and effort have been secured in analyzing the data. The new system permits all the radar data to be gathered in the digital computer in real time, thereby eliminating the need for post real-time processing of magnetic-tape recordings of the signals. Furthermore, it is now possible to transmit the data to other workers in computer-usable form.

This report describes the main functions of the computer program required to analyze the measurements, and lists the times of all measurements made with the new system prior to 1 January 1970. Examples of these results are presented and discussed.

14. KEY WORDS

Millstone radar
F-region
electron density
electron and ion temperatures
computer programming
magnetic-tape recording
ionospheric scatter
real-time processing